Organic Geochemistry 166 (2022) 104399

Contents lists available at ScienceDirect

Organic Geochemistry

journal homepage: www.elsevier.com/locate/orggeochem

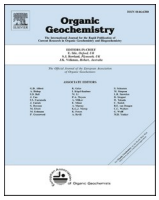

Identification, distribution and geochemical significance of dinaphthofurans in coals

Zhili Zhu [a,b], Meijun Li [a,c,*], Jiayang Li [a], Ling Qi [d], Xiaoqiang Liu [e], Hong Xiao [a], Junying Leng [b]

[a] State Key Laboratory of Petroleum Resources and Prospecting, College of Geosciences, China University of Petroleum, Beijing 102249, China
[b] State Key Laboratory of Shale Oil and Gas Enrichment Mechanisms and Effective Development, SINOPEC Key Laboratory of Petroleum Accumulation Mechanisms, Wuxi Research Institute of Petroleum Geology, Wuxi 214126, China
[c] Key Laboratory of Exploration Technologies for Oil and Gas Resources, Ministry of Education, College of Resources and Environment, Yangtze University, Wuhan 430100, China
[d] Research Institute of Petroleum Exploration and Development, PetroChina, Beijing 100083, China
[e] College of Chemistry and Environmental Engineering, Sichuan University of Science and Engineering, Zigong 643000, China

ARTICLE INFO

Associate Editor — **Kliti Grice**

Keywords:
Dinaphthofuran
Quantum chemical calculation
Thermodynamic stability
Maturity
Coal

ABSTRACT

All six dinaphthofuran (DNF) isomers have been unequivocally identified in sedimentary organic matter through the co-injection with commercially available standards for the first time. The elution order and retention indices (*I*) of dinaphthofurans (DNFs) were obtained by GC–MS analysis. Quantum chemical computations were carried out to determine the thermodynamic stability sequence of DNF isomers, which is as follows: dinaphtho[1,2-b;2′,1′-d]furan > dinaphtho[1,2-b;1′,2′-d]furan > dinaphtho[1,2-b;2′,3′-d]furan > dinaphtho[2,1-b;2′,3′-d]furan > dinaphtho[2,3-b;2′,3′-d]furan > dinaphtho[2,1-b;1′,2′-d]furan. The DNF isomers are ubiquitous in coal samples in this study. The effects of maturity on the distribution patterns of DNFs in the coals were investigated and the relative abundance of dinaphtho[1,2-b;2′,1′-d]furan (1221DNF) to dinaphtho[1,2-b;2′,3′-d]furan (1223DNF) is significantly controlled by maturation. Based on theoretical calculations and geochemical data, a dinaphthofuran maturity indicator, defined as DNFR (1221DNF/1223DNF), is proposed. A preliminary calibration of DNFR against the vitrinite reflectance (%Ro) was established with the following relationship: %Rc = 1.27 × DNFR – 1.12 (for %Ro values > 1.00). DNFR is a useful indicator in evaluating the maturity for sediments with Type II–III organic matter. DNFs in coals may be produced during diagenesis and catagenesis and oxic environment contributes to their generation. This study helps us better understand the occurrence and significance of complex oxygen-containing organic compounds in sedimentary organic matter.

1. Introduction

Dinaphthofurans (DNFs) are important complex oxygen-heterocyclic aromatic compounds in coal tar, oxidation products of coal, sediments, and sedimentary rocks (e.g. Borwitzky and Schomburg, 1979; Stock and Obeng 1997; Brack et al., 2003a, 2003b; Marynowski et al., 2009, 2011; Grafka et al., 2015). However, little is known about the detection, identification and geochemical significance of dinaphthofurans in petroleum geochemistry.

An unidentified dinaphthofuran isomer was first detected in coal-carbonization products by high-resolution mass spectrometry (Shultz et al., 1972) and in coal tar by GC–MS (gas chromatography-mass spectrometry) analysis (Borwitzky and Schomburg, 1979). Afterwards, four unidentified dinaphthofuran isomers were detected in oxidation and decarboxylation products of Pocahontas No. 3 Coal by GC–MS analysis (Stock and Obeng 1997). Brack et al. (2003a) tentatively identified all six dinaphthofuran isomers in sediments by high performance liquid chromatography (HPLC) and then Brack et al. (2003b) preliminarily identified two of the six dinaphthofuran isomers, namely dinaphtho[1,2-b;1′,2′-d]furan (1212DNF) and dinaphtho[2,1-b;2′,3′-d]furan (2123DNF), in contaminated sediments by mass spectra, retention index (*I*), reversed-phase liquid chromatography (RP–LC) capacity factors and UV absorption spectra. Subsequently, dinaphthofurans were detected and tentatively assigned in sediments by GC–MS, RP–HPLC and GC × GC-ToF-MS (Brack et al., 2005, 2007; Lübcke-von Varel et al., 2008; Skoczyńska et al., 2008; Xiao et al., 2016). Significantly,

* Corresponding author at: State Key Laboratory of Petroleum Resources and Prospecting, College of Geosciences, China University of Petroleum, Beijing 102249, China.
E-mail address: meijunli@cup.edu.cn (M. Li).

https://doi.org/10.1016/j.orggeochem.2022.104399
Received 6 November 2021; Received in revised form 27 February 2022; Accepted 1 March 2022
Available online 3 March 2022

Marynowski et al. (2009, 2011) and Grafka et al. (2015) tentatively detected some dinaphthofuran isomers in ancient sedimentary organic matter, but the specific positions of these isomers were not confirmed. Due to the potential biological carcinogenicity and mutagenicity (Vondráček et al., 2004), dinaphthofurans are important toxic pollutants in ecological environment and key research subjects in environmental and biological science (Brack et al., 2007; Skoczyńska et al., 2008; Xiao et al., 2016). However, up to now, there has been no report on the occurrence, identification, and distribution of dinaphthofurans in coals.

The origin of DNFs is still controversial. Poutsma and Dyer (1982) proposed that dinaphthofurans are the thermolysis products of naphthols. Guseva et al. (1980) reported that dinaphthofurans are major impurities in technical 2-naphthol. Brack et al. (2003b) thought that DNFs in sediments may be products of naphthol. Marynowski and

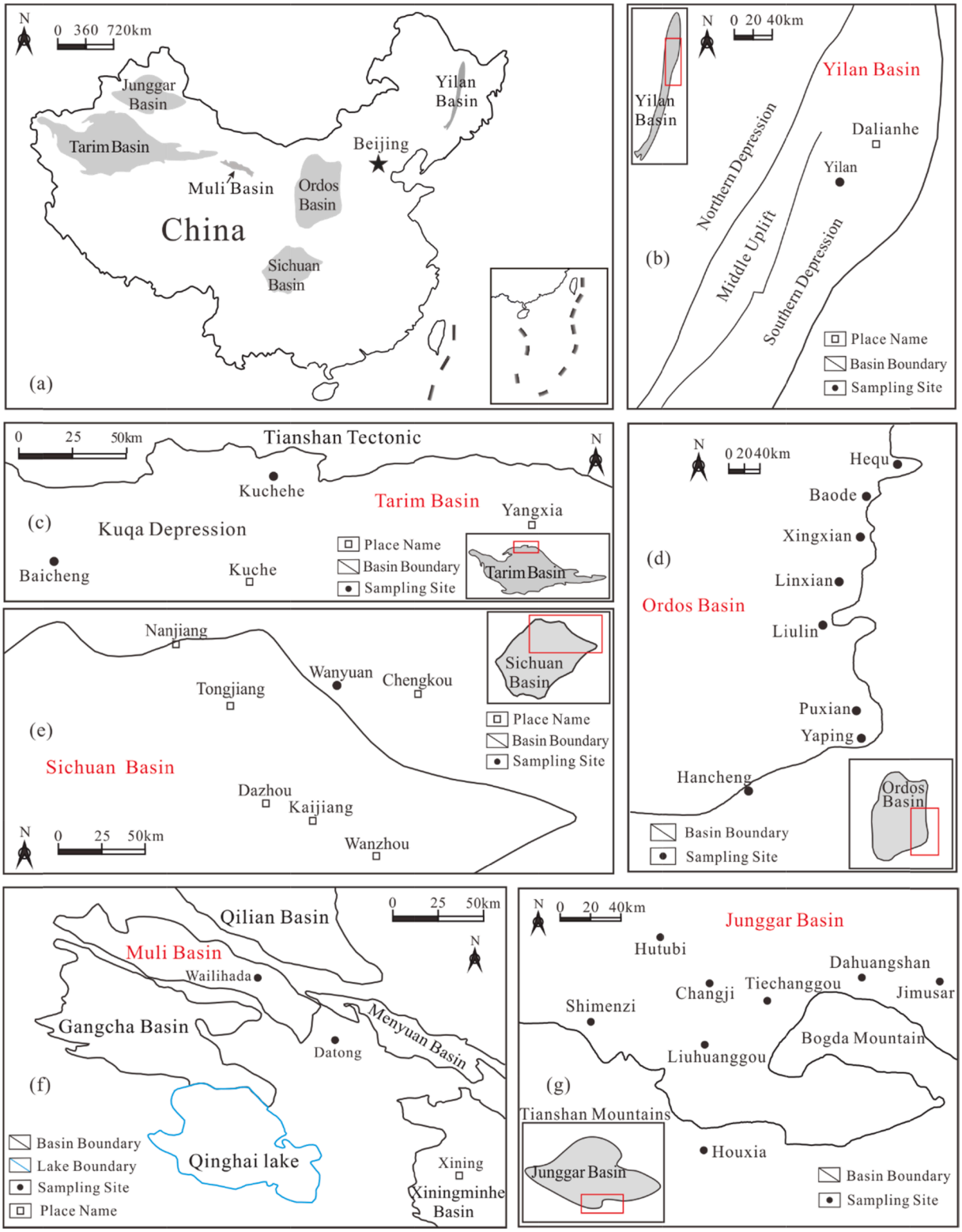

Fig. 1. Sampling sites of coals in the study (modified after Zhu et al., 2019).

Simoneit (2009) speculated that DNFs in charcoal-bearing sedimentary rocks may be derived from combustion processes. However, little work has been done to investigate the origin of DNFs in the geosphere.

Dibenzofuran (DBF), its methylated homologues (MDBFs), and benzo[b]naphthofurans (BNFs) are important oxygen-heterocyclic aromatic compounds and have been applied as useful molecular markers in organic geochemistry. The distribution patterns of DBF and MDBFs are mainly dependent on the depositional environment and organic matter type of source rock (Pu et al., 1991; Radke et al., 2000; Li et al., 2013; Li and Ellis, 2015). DBF and MDBFs seem to prevail in terrestrial and freshwater sedimentary rocks and coals (Pu et al., 1991; Li et al., 2013). The relative abundance of alkyldibenzofuran (ADBF) with respect to alkyldibenzothiophene (ADBT) has been proposed to distinguish depositional environments (Sephton et al., 1999; Kruge et al., 2000; Radke et al., 2000). More recently, researchers identified DBF, MDBFs and BNFs in crude oils and source rocks by comparison with co-injected internal standards, and suggested that they are potential molecular markers to indicate oil migration pathways and distances (Li et al., 2011; Li and Ellis, 2015).

The geochemical application and related formation mechanism of DNFs have not been reported. In this paper, all six dinaphthofuran isomers were unambiguously identified in sedimentary organic matter through co-injection of commercially available standards in GC–MS analyses for the first time. We calculated the standard retention indices of dinaphthofurans on a HP-5MS chromatographic column and present their mass spectra. Density functional theory (DFT) calculations were conducted to determine the thermal stability of each DNF isomer. We then depict the occurrence and distribution patterns of DNFs in coals from six different basins in China. A maturity indicator of dinaphthofurans is proposed based on geochemical data and theoretical calculations. The origin and formation mechanism of DNFs in the geosphere were also preliminarily investigated through comparison with dibenzofurans. This study attempts to provide a better understanding of the occurrence and source of dinaphthofurans in sedimentary organic matter.

2. Samples and geologic setting

The Junggar Basin, located in the northern Xinjiang Uygur Autonomous Region of China, is one of the important coal-producing basins in China (Fig. 1a,g) (Li et al., 2012; Fang et al., 2015). The coal seams mainly occur in Lower–Middle Jurassic sequence, including the Badaowan Formation (J_1b) and Xishanyao Formation (J_2x) (Chen et al., 2003; Qian et al., 2018). Fourteen coals were collected from J_1b and J_2x in the southeastern part of the basin. The Badaowan Formation mainly contains fluvial and paludal facies. The Xishanyao Formation was deposited in alternating environments of deltaic, fluvial, and lacustrine shores (Hendrix et al., 1995; Zhou et al., 2010). The Badaowan and Xishanyao formations were not affected by the hydrothermal activity (Liu et al., 2012).

The coals collected from the Junggar Basin are abundant in organic matter with total organic carbon (TOC) contents of 46.0–86.3%, hydrogen index (HI) values of 60.0–529 mg HC/g TOC, and extractable organic matter (EOM) of 16.3–95.2 mg/g C_{org}. The vitrinite reflectances ranges and Tmax values of most coals are 0.46–0.76 %Ro and 426–449 °C, respectively (Table 1). The organic matter is mainly comprised of Type II–III kerogen.

Ordos Basin is an intracratonic depression basin in north-central China (Fig. 1a,d) with the Paleozoic strata covering an area of 250 × 10^3 km^2 (Dai et al., 2005; Yang et al., 2005). The natural gas in Upper

Table 1
TOC contents, Rock-Eval pyrolysis analyses, vitrinite reflectances and extractable organic matter of the studied coal samples.

Basin	Sampling Site	Sample Name	Formation	Type	TOC (%)	Tmax (°C)	% Ro	HI (mg HC/g TOC)	OI (mg CO_2/g TOC)	EOM (mg/g C_{org})
Junggar Basin	Jimusar	JMSRS17	J_2x	Outcrop	46.0	432	0.53	419	16.1	95.2
		JMSRB6	J_2x	Outcrop	80.3	427	0.49	529	9.82	74.7
	Dahuangshan	DHSF10	J_1b	Outcrop	77.6	431	0.53	410	11.1	33.9
		DHSB2	J_1b	Outcrop	77.8	434	0.51	391	12.6	58.0
	Houxia	HXD1	J_1b	Outcrop	81.3	436	0.60	159	9.28	28.7
		HXB4	J_1b	Outcrop	80.5	428	0.53	430	9.44	35.7
	Hutubi	HTBA14	J_1b	Outcrop	78.5	434	0.50	198	11.3	25.9
		HTBA8	J_1b	Outcrop	82.0	444	0.68	98.7	8.58	22.8
		HTBA7	J_1b	Outcrop	86.3	454	1.08	60.0	7.99	20.7
	Changji	CJF5	J_1b	Outcrop	73.7	430	0.60	204	11.7	46.7
	Liuhuanggou	LHGE3	J_2x	Outcrop	71.4	431	0.52	87.9	18.6	16.3
		LHGE5	J_2x	Outcrop	71.5	426	0.46	221	21.0	34.1
	Shimenzi	SMZM1	J_2x	Outcrop	70.7	438	0.62	331	11.9	57.8
	Tiechanggou	TCGF7	J_2x	Outcrop	84.4	449	0.76	115	7.79	18.8
Ordos Basin	Baode	BDS24	C–P	Outcrop	68.6	444	0.62	246	8.85	74.3
		BDS14	C–P	Outcrop	73.9	444	0.71	236	8.69	71.8
	Linxian	LXS11	C–P	Outcrop	77.9	444	0.77	239	6.20	78.2
		LXS15	C–P	Outcrop	91.5	463	0.96	176	5.14	11.1
		LXS8	C–P	Outcrop	71.2	455	1.03	194	6.73	17.4
	Xingxian	XXS2	C–P	Outcrop	85.4	492	1.35	120	5.43	8.36
	Liulin	LLS25	C–P	Outcrop	84.3	493	1.40	97.4	4.45	7.84
		LLS5	C–P	Outcrop	75.1	489	1.27	96.9	4.09	15.1
	Hancheng	HCS1	C–P	Outcrop	80.7	498	1.66	62.9	4.38	2.69
		HCS4	C–P	Outcrop	83.8	501	1.88	48.8	4.12	4.78
	Puxian	PXS22	C–P	Outcrop	83.1	435	0.62	275	6.70	138
		PXS6	C–P	Outcrop	84.3	444	0.63	230	6.99	88.7
Tarim Basin	Baicheng	BCS16	J	Outcrop	88.3	491	1.81	54.8	2.42	4.58
	Baicheng	BCA1	J	Outcrop	76.8	448	1.18	200	4.00	36.09
	Kuchehe	KCA4	J	Outcrop	47.9	432	0.60	28.7	48.2	39.57
Sichuan Basin	Wanyuan	WY1	P	Outcrop	61.8	483	1.30	87.0	10.9	50.19
Muli Basin	Datong	DTG2	J	Outcrop	75.1	427	0.50	81.6	10.0	19.15
	Wailihada	WLG3	J	Outcrop	38.4	457	1.48	43.5	6.62	17.98
Yilan Basin	Yilan	YLF2	E	Outcrop	72.7	422	0.55	252	9.50	33.11
	Yilan	YLD4	E	Outcrop	66.9	435	0.59	191	6.50	6.77

TOC: total organic carbon; Tmax: temperature at maximum generation; %Ro: vitrinite reflectance; HI: hydrogen index = $S_2 \times 100/TOC$; OI: oxygen index = $S_3 \times 100/TOC$; EOM: extractable organic matter.

Paleozoic strata was mainly derived from the Carboniferous–Permian (C–P) coal measure source rocks and coals (Dai et al., 2005; Hu et al., 2010). These source rocks were widely distributed over the entire basin and have an area of 180 × 10^3 km^2 (Shuai et al., 2013; Huang et al., 2015). The Carboniferous–Permian stratum principally developed marine–terrestrial transitional facies and consists of coal seams, black shales, and sandstones. The Upper Palaeozoic strata were affected by hydrothermal fluid alteration due to the volcanic activity, which occurred in the Early Cretaceous in the southeast of the Ordos Basin (Yang et al., 2005; Li and Gao, 2010). A suite of 12 coal samples were collected from Carboniferous–Permian coal measure strata in this basin. The TOC, HI, and extractable organic matter values of the coals are 68.6–91.5%, 48.8–275 mg HC/g TOC, and 2.69–138 mg/g C_{org}, respectively. Based on the Tmax and HI values, the coals mainly contain Type II–III kerogen. Most coals from this basin are characterized by higher maturity with %Ro = 0.96–1.88 (Table 2).

The Tarim Basin, in northwestern China, is the largest inland basin and one of the most important hydrocarbon-producing basins in China (Li et al., 1996). The Kuqa Depression is located in the northern part of the Tarim Basin (Fig. 1a,c). The Jurassic strata contains many thick coal beds, which were deposited in lacustrine and marginal lacustrine–swamp transitional environments (Liang et al., 2003; Jia and Li, 2008). Three coal samples were collected from the Jurassic formation. The coals have TOC, HI, Tmax and EOM values of 47.9–88.3%, 28.7–200 mg HC/g TOC, 432–491 °C and 4.58–39.6 mg/g C_{org}, respectively. Based on the Tmax and HI values, these coals mainly contain Type II–III kerogen. The coals from this basin are characterized by higher maturity with %Ro = 0.60–1.81 (Table 1).

The Yilan Basin, located in northeastern China, is a typical Cenozoic faulted basin (Fig. 1a,b). The coal seams mainly occur in Paleogene strata, which were deposited in lacustrine and delta facies (Liu et al., 2012; Wang et al., 2013). Two coal samples were collected from the Paleogene formation. The Muli Basin, located in the north of Qinghai Province, China, is a coal-rich sedimentary basin (Fig. 1a,f). The coal seams occur mainly in Jurassic strata, and the sedimentary environments are mainly lacustrine, swamp and deltaic (Zhang, 1996; Xu et al., 2011). Two coal samples were collected from the Jurassic formation. The Sichuan Basin, located in the northwest of the Yangtze Platform, is a large superimposed basin (Fig. 1a,e) (Zou et al., 2014; Zhu et al., 2015). The Upper Permian formation is a set of coal-bearing strata distributed in the northeast of the Sichuan Basin, which were mainly deposited in a marine–terrestrial transitional sedimentary environment (Feng et al., 2013; Tenger et al., 2013). One coal sample was collected from the Permian formation. The coals from the above three basins have TOC, HI, EOM values of 38.4–75.1%, 43.5–252.5 mg HC/g TOC, 6.77–50.1 mg/g C_{org}, respectively (Table 1). The coals are low mature to high mature with vitrinite reflectances of 0.50–1.48 %Ro and Tmax values of 422–483 °C. These geochemical characteristics indicate that the coals consist of Type II–III kerogen.

3. Analytical methods and reference standards

3.1. Analytical methods

A Leica MPV-SP microphotometer was used to measure the vitrinite reflectances (%Ro) on the polished coals according to the method of Kilby (1988). The TOC contents were determined by Carbon/Sulfur Analyzer (LECO CS-230). The OGE-VI Pyrolysis Apparatus was used to

Table 2
Concentrations of dinaphthofurans and dibenzofurans in coal samples.

Sample Name	C_{29} ααα 20S/(20S + 20R) sterane	C_{31} 22S/(22S + 22R) hopane	Pr/Ph	F_1	F_2	DNFR	4-MDBF/1-MDBF	DBFs (μg/g C_{org})	DNFs (μg/g C_{org})
JMSRS17	0.27	0.58	5.95	0.21	0.15	0.18	0.83	0.02	0.32
JMSRB6	0.31	0.61	5.98	0.17	0.12	0.24	0.97	0.01	0.90
DHSF10	0.24	0.56	4.63	0.36	0.27	0.23	1.79	0.01	0.39
DHSB2	0.25	0.60	3.66	0.39	0.28	0.27	1.60	0.01	0.86
HXD1	0.19	0.52	7.13	0.31	0.18	0.16	1.31	0.01	1.95
HXB4	0.27	0.60	7.53	0.14	0.09	0.18	0.93	0.02	1.24
HTBA14	0.20	0.51	10.30	0.35	0.21	0.17	0.76	0.05	2.96
HTBA8	0.29	0.57	5.06	0.43	0.25	0.20	0.78	0.06	2.31
HTBA7	0.28	0.54	3.13	0.52	0.29	0.20	0.63	0.15	2.13
CJF5	0.21	0.55	7.69	0.35	0.21	0.20	0.68	0.20	3.22
LHGE3	0.27	0.36	9.80	0.41	0.27	0.17	1.06	0.02	1.07
LHGE5	0.20	0.29	4.07	0.26	0.16	0.08	0.57	0.06	0.43
SMZM1	0.29	0.62	7.74	0.28	0.16	0.23	0.58	0.95	0.85
TCGF7	0.37	0.59	8.85	0.34	0.20	0.25	0.43	0.68	2.11
BDS24	0.42	0.58	0.77	0.45	0.25	0.26	1.35	0.34	0.62
BDS14	0.41	0.59	0.99	0.48	0.26	0.30	1.92	0.85	0.65
LXS11	0.41	0.62	1.41	0.50	0.28	0.11	0.96	3.38	0.64
LXS15	0.40	0.59	1.47	0.54	0.31	0.10	1.76	4.66	0.26
LXS8	0.48	0.58	0.96	0.55	0.31	0.09	1.54	3.35	0.33
XXS2	0.41	0.59	1.39	0.77	0.44	0.85	0.52	0.66	0.14
LLS25	0.46	0.56	1.20	0.78	0.44	0.83	0.27	0.41	0.13
LLS5	0.43	0.56	1.14	0.77	0.43	0.68	0.39	0.15	0.09
HCS1	0.43	0.61	0.77	0.87	0.53	1.09	0.42	0.24	0.24
HCS4	0.40	0.53	0.70	0.87	0.52	1.31	0.40	0.06	0.18
PXS22	0.47	0.59	1.40	0.47	0.26	0.18	1.62	2.24	0.85
PXS6	0.45	0.59	1.10	0.48	0.26	0.16	2.04	3.78	0.96
BCS16	0.51	0.57	2.13	0.73	0.41	0.96	0.75	0.01	0.27
BCA1	0.41	0.59	3.81	0.45	0.32	0.23	1.11	0.04	1.06
KCHA4	0.21	0.57	5.62	0.52	0.34	0.36	0.35	0.07	1.11
WY1	0.36	0.56	0.83	0.53	0.32	0.44	0.56	3.23	0.96
DTG2	0.40	0.24	6.54	0.31	0.16	0.09	0.86	0.01	1.90
WLG3	0.38	0.58	6.21	0.52	0.27	0.58	0.59	0.21	0.76
YLF2	0.13	0.53	6.63	0.29	0.20	0.10	0.27	0.07	0.62
YLD4	0.24	0.58	4.53	0.42	0.26	0.32	0.49	0.03	0.31

Pr/Ph: pristane/phytane; F_1: (3-MP + 2-MP)/(1-MP + 2-MP + 3-MP + 9-MP); F_2: (2-MP)/(1-MP + 2-MP + 3-MP + 9-MP); DNFR: 1221DNF/1223DNF; DNFs: the sum of the absolute concentrations of 1221DNF, 2112DNF, 1212DNF, 1223DNF, 2123DNF, and 2323DNF; DBFs: the sum of the absolute concentrations of 1-, 2-, 3-, 4-methyldibenzofuran and dibenzofuran.

obtain the Rock-Eval pyrolysis parameters (Zhu et al., 2019). Prior to analysis, deionized water and HCl were added to the coal samples for removing contaminants and dissolving carbonates, respectively.

The coals were ground into powder (< 0.18 mm). The powder samples were extracted with 400 ml dichloromethane/methanol (93:7, v/v) for 48 h in a Soxhlet apparatus to obtain soluble bitumen. The extracts were deasphalted with petroleum ether, and then separated into saturated, aromatic and resin fractions by liquid chromatography on a column of alumina/silica gel. The eluents were petroleum ether, dichloromethane/petroleum ether (2:1, v/v), and dichloromethane/methanol (93:7, v/v), respectively. Saturated, aromatic fractions, and mixture standards were analyzed by GC–MS on an Agilent 5975i GC–MS

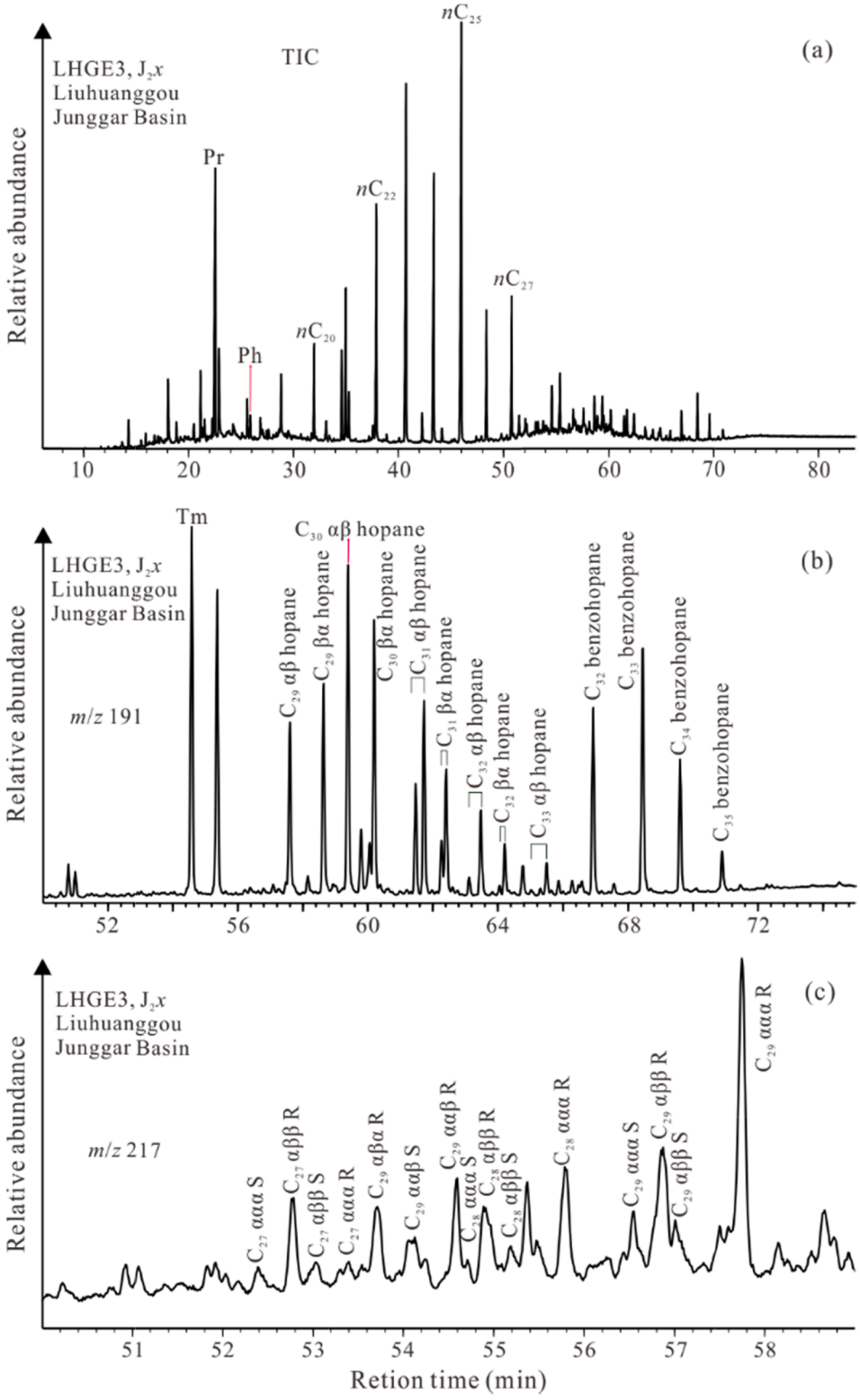

Fig. 2. (a) Total ion current chromatogram, (b) mass chromatograms *m/z* 191 and (c) *m/z* 217 of the aliphatic fraction from coal extract. ααα and αββ denote 5α(H),14α(H),17α(H)-sterane and 5α(H),14β(H),17β(H)-sterane, respectively.

system equipped with a HP-5MS (5% phenylmethylpolysiloxane) fused quartz capillary column (60 m × 0.25 mm i.d., 0.25 μm film thickness). The GC oven programming for aromatic components began at 80 °C, which was held for 1 min, then raised to 310 °C at 3 °C/min and held isothermal for 16 min. For saturated fractions, the GC temperature program was as follows: the initial temperature of the oven was kept at 50 °C for 1 min, increased to 120 °C at 20 °C/min, then ramped to 310 °C at the rate of 3 °C/min, and finally was kept constant for 25 min. The carrier gas was helium and the injector temperature was 300 °C. The mass spectromterused electron impact (EI) with ionization energy of 70 eV and scanning range of 50–600 Da.

3.2. Reference standards

Six commercially available standards of dinaphthofuran isomers, i.e., dinaphtho[1,2-b;2′,1′-d]furan (1221DNF), dinaphtho[2,1-b;1′,2′-d]furan (2112DNF), dinaphtho[1,2-b;1′,2′-d]furan (1212DNF), dinaphtho[1,2-b;2′,3′-d]furan (1223DNF), dinaphtho[2,1-b;2′,3′-d]furan (2123DNF), and dinaphtho[2,3-b;2′,3′-d]furan (2323DNF), were purchased from Chiron AS, Norway. In order to calculate the retention indices of dinaphthofuran isomers, we added picene, chrysene, and phenanthrene to mixture solutions of authentic standards as markers.

3.3. Quantification of polycyclic aromatic hydrocarbons (PAHs)

A known amount of deuterium-substituted phenanthrene (phenantharene-d_{10}; molecular formula: $C_{14}D_{10}$; molecular mass: 188) was added to each sample as an internal standard prior to GC–MS analysis. The peak of phenantharene-d_{10} can be identified on m/z 188 mass chromatogram, which is just eluted before the phenanthrene peak. The peak area of DBF, MDBFs and DNFs were determined on m/z 168, 182, and 268 mass chromatograms. By correlation with the peak area of phenantharene-d_{10}, the concentrations of DBF, MDBFs and DNFs can be calculated.

4. Results and discussion

4.1. Distributions of aliphatic and aromatic hydrocarbons in coals

The total ion current (TIC) of the aliphatic fraction of the coal extract (Fig. 2a) is dominated by a series of *n*-alkanes ranging from C_{14} to C_{30}. The distributions of *n*-alkanes are relatively similar in most the coal samples. Long chain C_{21}–C_{27} *n*-alkanes are characterized by an odd-over-even predominance with a maximum at *n*-C_{25}. Pristane and phytane were also detected in the coals. The Pr/Ph ratios of the coals from the Junggar, Tarim, Muli, and Yilan basins range from 2.13 to 10.3, while the coals from the Ordos and Sichuan basins were at the range of 0.70–1.47 (Table 2). Series of αβ-hopanes are dominated by 17α(H),21β(H)-hopanes (22R and 22S epimers) from C_{29} to C_{33}, with a maximum at C_{30} hopane (Fig. 2b). Series of βα-moretanes (17β(H),21α(H)-hopanes) were also detected ranging from C_{29} to C_{32}, with a maximum at C_{30}. C_{27} 17α(H)–22,29,30-trisnorhopane (Tm) was present in the coals with high abundance (Fig. 2b). C_{27} 18α(H)–22,29,30-trisnorneohopane (Ts), oleanane and gammacerane were present in very low concentration or absent in the coals. C_{32}–C_{35} benzohopanes were also detected in the coals, which were reported in source rocks and coals in previous studies (e.g., Liao et al., 2015; Nytoft et al., 2016). Steranes are dominated by the C_{29} 5α(H),14α(H),17α(H)-20R regular sterane (C_{29} ααα 20R sterane), followed by an important contribution of the αββ isomer (Fig. 2c). The C_{27}–C_{29} steranes of most of the samples exhibit a $C_{29} > C_{28} > C_{27}$ steranes distribution pattern.

Fig. 3 displays the partial TIC of the aromatic fractions from the coal sample and the main constituents are assigned. Alkylnaphthalene, alkylphenanthrenes and 4- to 6-rings polycyclic aromatic hydrocarbons (PAHs) are the most abundant compounds observed in the aromatic fractions of the coals. Dibenzofuran (DBF), alkyldibenzofurans (MDBF, DMDBF), and dinaphthofurans (DNFs) were also detected in the aromatic fractions, and their elution sequence is as follows: DBF, MDBFs, DMDBFs, DNFs.

4.2. Identification of the dinaphthofurans

Some dinaphthofuran isomers in the pyrolysates of coal, sediments, and sedimentary organic matter have been tentatively assigned without co-injection of authentic standards (Stock and Obeng 1997; Brack et al., 2003a, 2003b, 2005, 2007; Marynowski et al., 2009, 2011). The unequivocal identification of dinaphthofurans in ancient sedimentary rocks has not yet been achieved. All six dinaphthofuran isomers were firmly identified in the coal extracts using the co-injection of authentic standards.

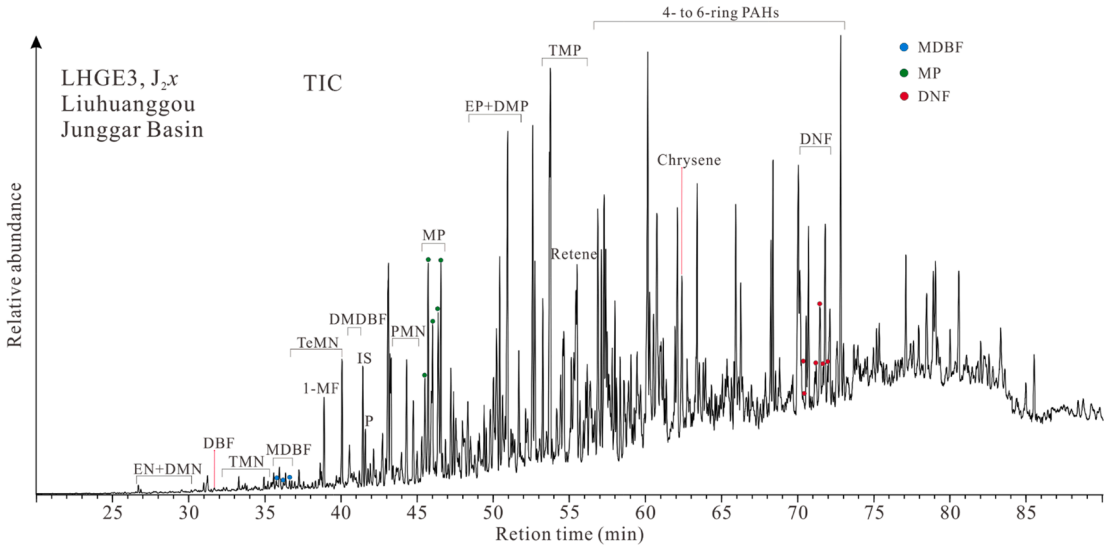

Fig. 3. Total ion current chromatogram of the aromatic fractions from coal extract. Abbreviations: EN + DMN: ethyl- and dimethylnaphthalene; DBF: dibenzofuran; TMN: trimethylnaphthalene; MDBF: methyldibenzofuran; TeMN: tetramethylnaphthalene; 1-MF: 1-methyl fluorene; DMDBF: dimethyldibenzofuran; IS: internal standard; P: phenanthrene; PMN: pentamethylnaphthalene; MP: methylphenanthrene; EP + DMP: ethyl- and dimethylphenanthrene; TMP: trimethylphenanthrene; PAHs: polycyclic aromatic hydrocarbons.

The retention index system has been used to compare the retention behavior of the compounds usingdifferent chromatographic columns (Kovats, 1958; van den Dool and Kratz, 1963). The retention index markers for PAHs analyses are phenanthrene (three rings, I = 300), chrysene (four rings, I = 400), and picene (five rings, I = 500) (Lee et al., 1979; Li et al., 2012; Zhu et al., 2019). The formula reported by Lee et al. (1979) was used in this study to calculate the retention indices of the dinaphthofuran isomers. By co-injection of commercially available standards, the elution order and retention indices of the six dinaphthofuran isomers could be unequivocally determined. The elution sequence of the dinaphthofurans using a HP-5MS capillary column is follows: 1221DNF, 2112DNF, 1212DNF, 1223DNF, 2123DNF, and 2323DNF (Fig. 4), which is similar to the result of Brack et al. (2003b). However, the measured retention indices for 1212DNF and 2123DNF in this study (Table 3) are a little higher than that calculated by Brack et al. (2003b).

Fig. 5 shows the background subtracted mass spectra of six dinaphthofuran isomers. All isomers are characterized by the highest abundance of the molecular ion M^+ at m/z 268. The mass spectra of dinaphthofurans have diagnostic ion fragments at m/z 239, 134, 120 and 106 with high abundance of doubly charged ion at m/z 134. The mass spectra of 1221DNF, 1212DNF, 1223DNF, 2123DNF, and 2323DNF are quite similar (Fig. 5a,c–f). The essential difference between the five isomers (1221DNF, 1212DNF, 1223DNF, 2123DNF, and 2323DNF) and the other (2112DNF) is in the relative abundances of m/z 120 and m/z 239 ions relative to m/z 134 and m/z 268, respectively. For 1221DNF, 1212DNF, 1223DNF, 2123DNF, and 2323DNF, the m/z 120 and m/z 239 ion fragments are relatively low with the 120/134 ratios of 54–85% and 239/268 ratios of 17–24% (Fig. 5a,c–f). In contrast, 2112DNF has high abundances of the m/z 120 and 239 ions with a 120/134 value of 405%, and a 239/268 value of 33%, respectively (Fig. 5b). It appears that the isomer (2112DNF) tends to fragment more easily, indicating its low thermal stability. For the 2112DNF, the intensities of the double-charged ions m/z 133 and 134 are similar (Fig. 5b). However, for the 1221DNF, 1212DNF, 1223DNF, 2123DNF, and 2323DNF, the intensity of m/z 133 ion is much lower than that of m/z 134 ion (Fig. 5a, c–f).

4.3. Thermodynamic stabilities of the dinaphthofuran isomers

The DFT calculations has become an important tool for studying geochemical phenomena at the molecular level (e.g., Xiao et al., 2019; Zhu et al., 2019; Liu et al., 2020; Wang et al., 2020). We conducted quantum chemical calculations to obtain the thermodynamic

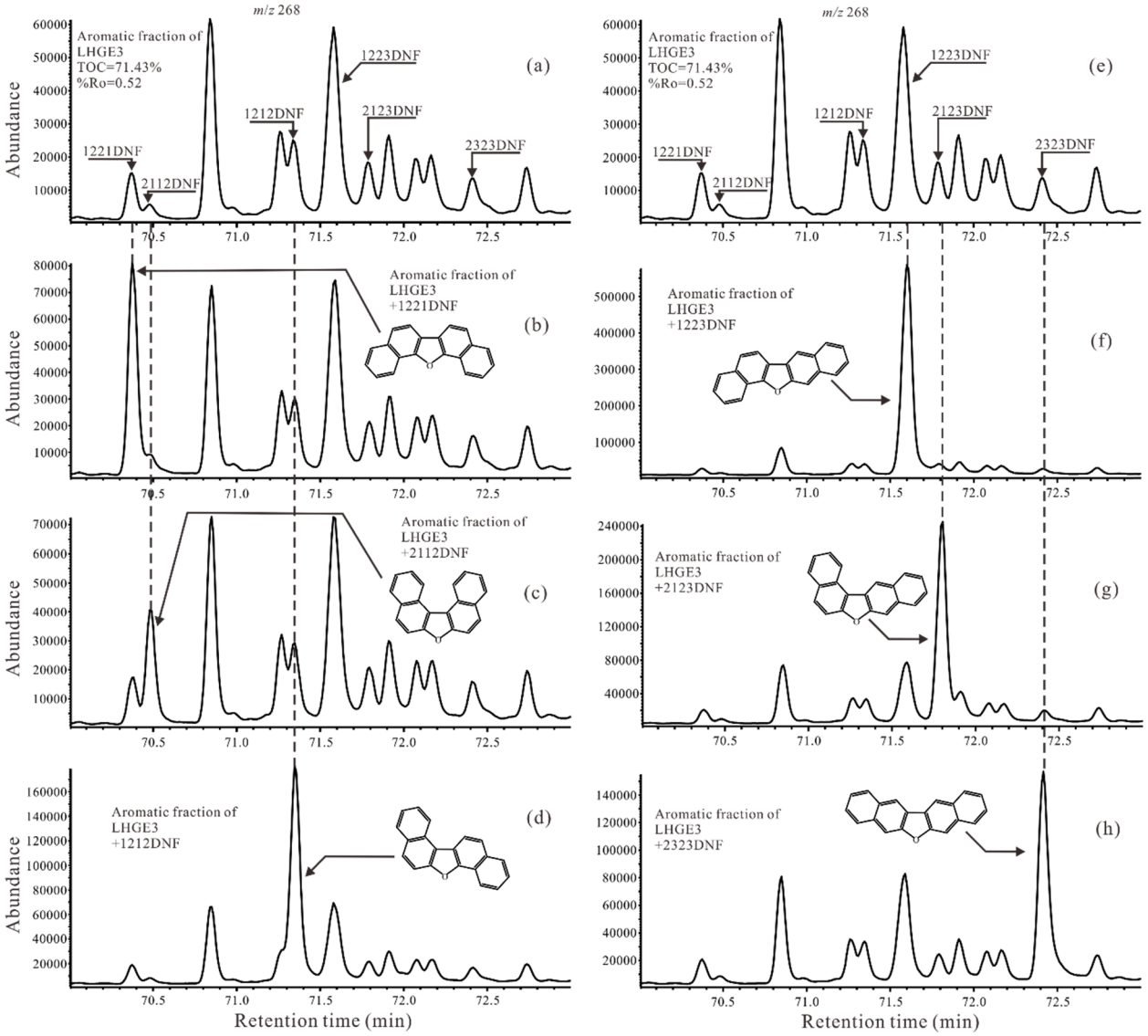

Fig. 4. Identification of the dinaphthofurans in the coal of this study.

Table 3
Retention indices of dinaphthofurans.

Compounds	Reference (HP-5MS)[a]	Authentic standards (HP-5MS)		Coal, Ordos Basin (HP-5MS)		Coal, Junggar Basin (HP-5MS)		Identification
	I	t_R	*I*	t_R	*I*	t_R	*I*	
Phenanthrene	300.00	41.886	300.00	41.864	300.00	41.850	300.00	Phenanthrene
Chrysene	400.00	62.615	400.00	62.536	400.00	62.537	400.00	Chrysene
dinaphtho[1,2-b;2′-1-d]furan	–	70.414	444.26	70.352	444.36	70.370	444.49	dinaphtho[1,2-b;2′-1-d]furan
dinaphtho[2,1-b;1′-2′-d]furan	–	70.509	444.80	70.395	444.61	70.481	445.12	dinaphtho[2,1-b;1′-2′-d]furan
dinaphtho[1,2-b;1′-2′-d]furan	440.10	71.389	449.79	71.300	449.74	71.339	449.99	dinaphtho[1,2-b;1′-2′-d]furan
dinaphtho[1,2-b;2′-3′-d]furan	–	71.638	451.20	71.514	450.96	71.581	451.36	dinaphtho[1,2-b;2′-3′-d]furan
dinaphtho[2,1-b;2′-3′-d]furan	447.40	71.832	452.30	71.813	452.66	71.787	452.53	dinaphtho[2,1-b;2′-3′-d]furan
dinaphtho[2,3-b;2′-3′-d]furan	–	72.501	456.10	72.391	455.94	72.412	456.08	dinaphtho[2,3-b;2′-3′-d]furan
Picene	500.00	80.237	500.00	80.154	500.00	80.145	500.00	Picene

t_R:retention time; *I*: retention index.
[a] retention indices of dinaphthofurans according to Brack et al. (2003b).

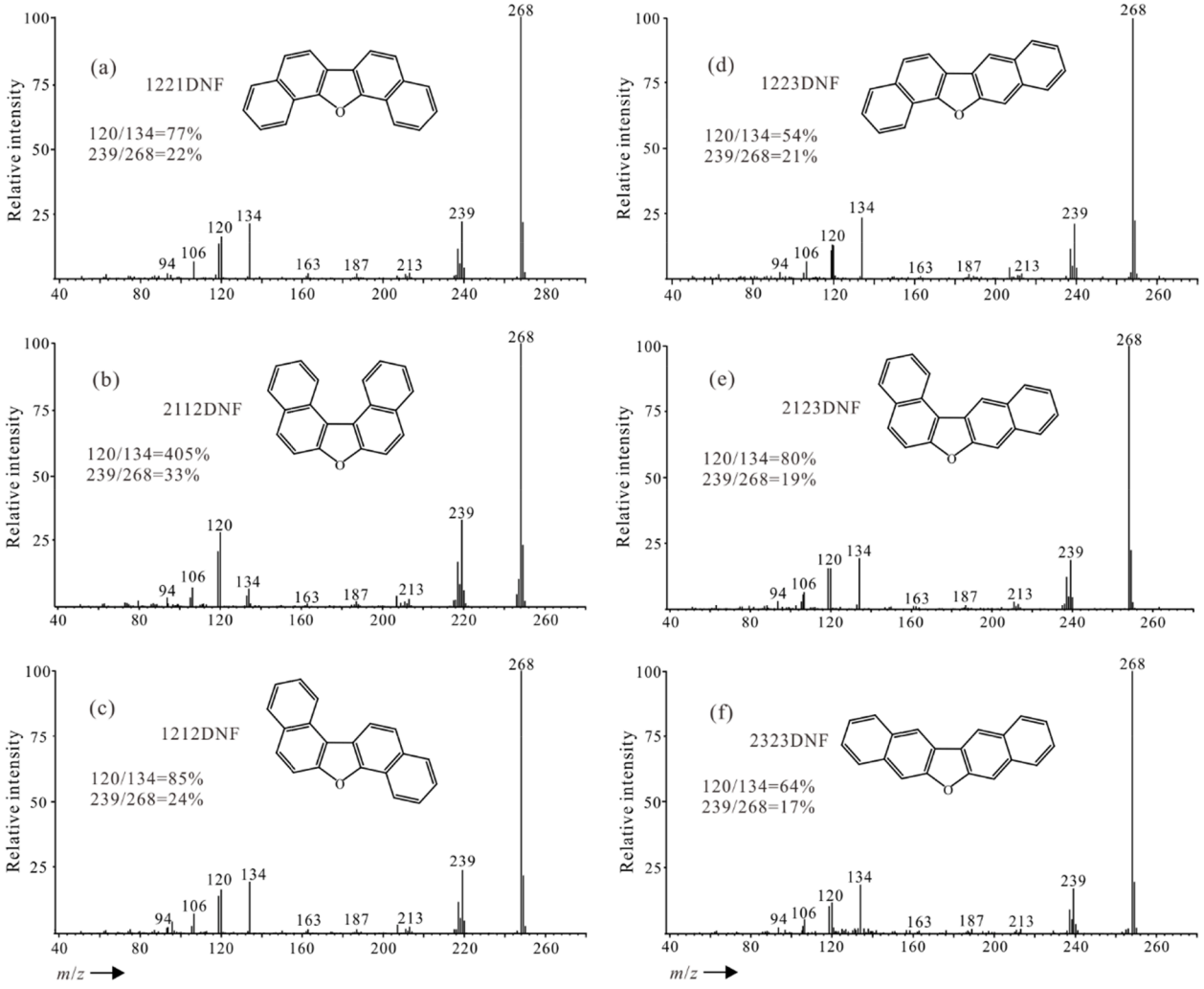

Fig. 5. Mass spectra of authentic dinaphthofuran isomers ordered in their elution sequence on an HP-5MS column.

parameters, such as Gibbs free energy (ΔG), internal energy (ΔU), electron energy (ΔE), and enthalpy (ΔH), of DNFs. Gaussian 09 software was used for all DFT calculations in this study (Zhu et al., 2019; Liu et al., 2020). The geometries optimized in the gas phase at 25 °C were carried out using the computing method of B3LYP/6–311++G (d,p) (Zhu et al., 2019; Liu et al., 2020).

The calculations of thermodynamic properties of the dinaphthofuran isomers show that 2112DNF has the highest energy, suggesting it is the least stable isomer. However, 1221DNF is the most stable isomer with the lowest energy. The thermodynamic stabilities of six dinaphthofuran isomers decrease following the order: 1221DNF > 1212DNF > 1223DNF > 2123DNF > 2323DNF > 2112DNF (Table 4). Previous studies have reported that steric hindrance may be an important control factor of thermodynamic stability and Gibbs free energy for aromatic compounds (Yang et al., 2019; Zhu et al., 2019; Liu et al., 2020). The steric hindrance of the two naphthalene rings at furan ring cause the thermodynamic instability (Fig. 6). For 2112DNF, these angles between the naphthalene rings and the furan ring are considerably deformed

Table 4
Thermodynamic properties of dinaphthofurans.

Isomer	△E (kcal/mol)	△U (kcal/mol)	△H (kcal/mol)	△G (kcal/mol)
dinaphtho[1,2-b;2′-1′-d]furan	0.00	0.00	0.00	0.00
dinaphtho[1,2-b;1′-2′-d]furan	0.73	0.74	0.74	0.70
dinaphtho[1,2-b;2′-3′-d]furan	1.53	1.55	1.55	1.47
dinaphtho[2,1-b;2′-3′-d]furan	2.20	2.23	2.23	2.10
dinaphtho[2,3-b;2′-3′-d]furan	2.43	2.44	2.44	2.45
dinaphtho[2,1-b;1′-2′-d]furan	6.83	6.80	6.80	6.92

from the optimal 120° (Fig. 6b). This makes the total energy increase and causes the instability. For comparison, these corresponding angles for 1221DNF, 1212DNF, 1223DNF, 2123DNF and 2323DNF, the more stable isomers, are less deformed.

4.4. *Effects of maturity on the distribution patterns of the dinaphthofurans*

Some dinaphthofuran isomers have been detected in the products of coal chemical industry (e.g., coal tar and coal pyrolysates) and sediments (Shultz et al., 1972; Borwitzky and Schomburg, 1979; Brack et al., 2003a,b). Afterwards, dinaphthofurans were tentatively detected in Triassic mudstones, Jurassic fossil wood, and Silurian shales from Poland (Marynowski et al., 2009, 2011; Grafka et al., 2015). In this study, dinaphthofurans were detected in the Jurassic coals from Junggar and Tarim basins, Carboniferous–Permian coals from Ordos and Muli basins, and Paleogene coals from Yilan Basin. These reports of dinaphthofurans indicate the wide occurrence of DNFs in the sedimentary organic matter. Fig. 7 shows the distribution patterns of the dinaphthofurans in the coals with different thermal maturities. Less mature coals with %Ro = 0.53–1.08 contain 1223DNF as the dominant isomer and have relatively low abundances of 1221DNF, 1212DNF, and 2123DNF, while 2112DNF and 2323DNF are present in very low concentrations (Fig. 7a–c). For highly mature coals (≥ 1.27 %Ro), the abundance of 1221DNF is high and comparable to that of 1223DNF, while 1212DNF, 2123DNF and 2323DNF occur in relatively low abundances and 2112DNF is below the detection limit or absent. The concentrations of 2112DNF are minor in less mature coals and become essentially absent at high thermal maturities, suggesting that 2112DNF is the least stable isomer, which is consistent with the results of our theoretical calculations. Obviously, compared with 1223DNF, the concentrations of 1221DNF display an overall increase with increasing maturity. Based on the distribution patterns of the DNFs in the coals, the thermal maturity is the main control factor of the relative abundances of 1221DNF and 1223DNF. It can be reasonably estimated that the thermodynamic stability of 1223DNF is lower than that of 1221DNF, which is in accord with the calculated thermal stability sequence.

Based on theoretical calculations and geochemical data, a thermal maturity parameter of DNFs, defined as DNFR (1221DNF/1223DNF), is

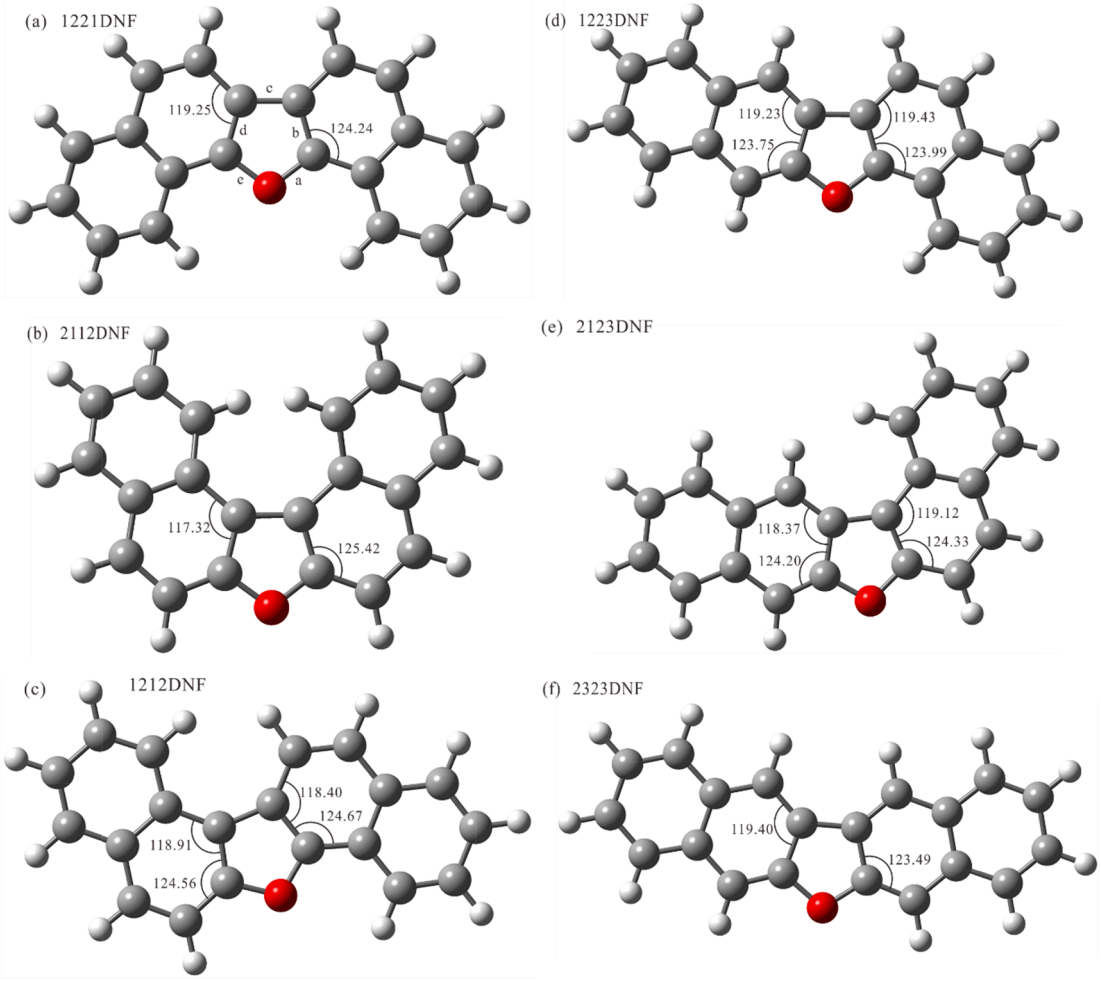

Fig. 6. The geometric optimizations of: (a) 1221DNF, (b) 2112DNF, (c) 1212DNF, (d) 1223DNF, (e) 2123DNF, and (f) 2323DNF.

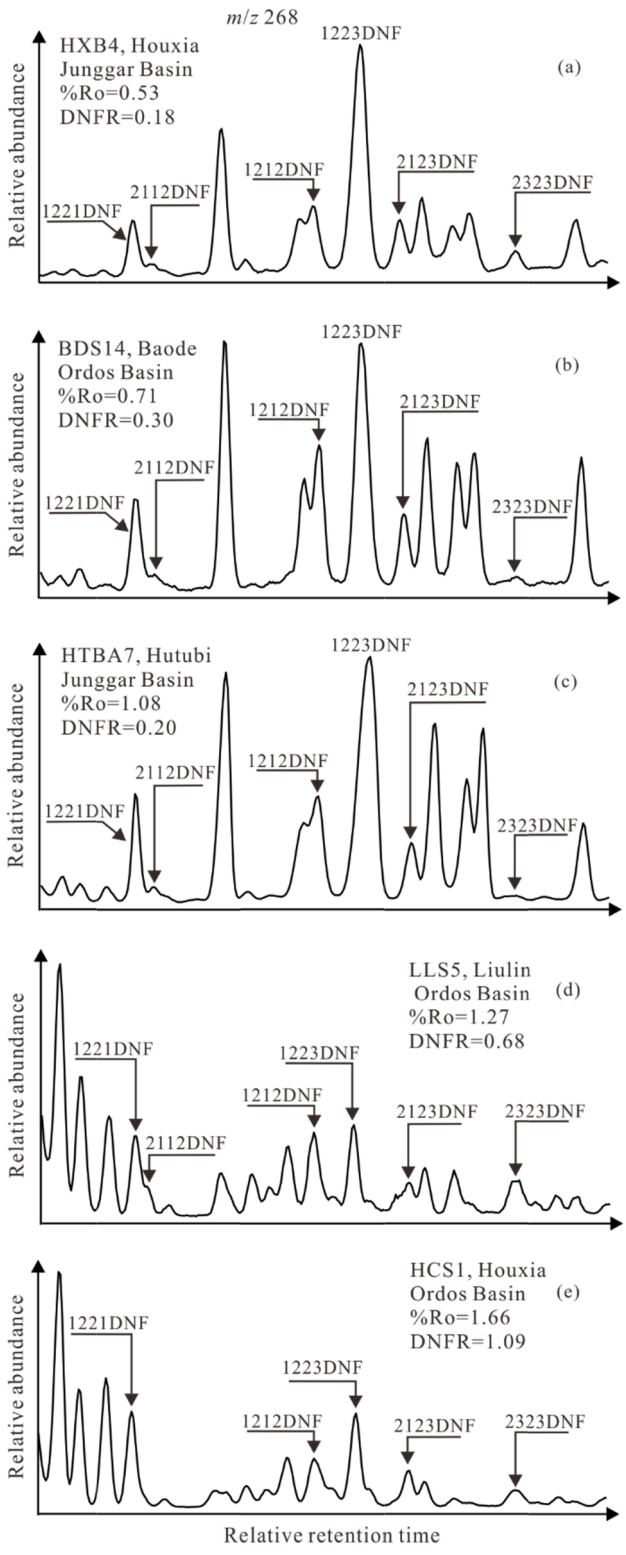

Fig. 7. Distribution patterns of dinaphthofurans in the coals with different thermal maturities.

proposed. Fig. 8a illustrates that DNFR (dinaphthofuran ratio) values display a generally increase with an increase in thermal maturity. For the coals with %Ro = 0.46–0.96, the DNFR ratios keep a low, nearly constant value. Then they gradually increase with the increase of thermal maturity after the peak of oil generation (> 1.03 %Ro). Previous studies suggested that the distribution patterns of PAHs are usually kinetically controlled at low thermal maturity and it can be also thermodynamically controlled at more advanced stages of maturity, depending on the specific PAHs stability (van Duin et al., 1997; Rospondek et al., 2009). The increasement of DNFR values in this study suggested an increase in the concentration of the more thermally stable isomer (1221DNF) and a decrease in the concentration of the less thermally stable isomer (1223DNF) after the peak of oil generation (> 1.03 %Ro). This is related to the formation mechanism of DNFs. The less stable isomer (e.g., 1223DNF) tends to be generated at the low maturity stage (Yang et al., 2017; Zhu et al., 2019; Liu et al., 2020). With an increase in thermal maturity, the isomer with low thermal stability (e.g., 1223DNF) is likely to degrade or may transform into the isomer with higher thermal stability (e.g., 1221DNF). Thus, compared with 1223DNF, the concentration of 1221DNF increases with the increase of thermal maturity. Fig. 8a illustrates that DNFR has a good linear relationship with the vitrinite reflectance at %Ro = 1.03–1.88. A calibration of DNFR against %Ro in the range of 1.03–1.88% was thus preliminarily established. The specific formula is: %Rc = 1.27 × DNFR – 1.12 (for values of %Ro > 1.0) with the related coefficient (R^2) up to 0.86. This indicates that dinaphthofurans are useful in petroleum geochemistry as molecular markers, and DNFR is a potential maturity indicator at high maturity stages.

4.5. *Relationships between dinaphthofuran ratio and selected molecular maturity parameters*

The C_{31} 22S/(22S + 22R) hopane ratio is an effective maturity indicator for immature to the early oil generation stages, whilst ratios in the range of 0.57–0.62 suggest that the main phase of oil generation has been reached or surpassed (Seifert and Moldowan, 1980; Peters et al., 2005). The C_{29} ααα 20S/(20S + 20R) sterane ratio proposed by Seifert and Moldowan (1986) is a commonly used biomarker maturity parameter which reaches equilibrium at 0.52–0.55. As can be seen from Fig. 9a, DNFR values for the coals remain at a low constant value at C_{31} 22S/(22S + 22R) hopane ratios of 0.24–0.57. However, DNFR values show an increase when C_{31} 22S/(22S + 22R) hopane ratio reaches the equilibrium value (0.57–0.62). The trend of DNFR values with increasing C_{29} ααα 20S/(20S + 20R) sterane ratios is similar to that of the C_{31} 22S/(22S + 22R) hopane.

The DNFR values for the coals remain at a low constant value at C_{29} ααα 20S/(20S + 20R) sterane ratios = 0.14–0.42. DNFR values also exhibit an increase with C_{29} ααα 20S/(20S + 20R) sterane ratios = 0.42–0.51. Interestingly, for most of the coal samples with high maturity (> 1.0 %Ro), C_{29} ααα 20S/(20S + 20R) sterane ratios (0.42–0.51) are lower than the equilibrium values (0.52–0.55). The reason may be that high maturities cause the decrease of C_{29} ααα 20S/(20S + 20R) sterane ratios (Peters et al., 1990). The results are consistent with the trend of DNFR values with increasing vitrinite reflectances, which suggest that DNFR values have wider validity as maturity parameter compared with C_{29} ααα 20S/(20S + 20R) sterane and C_{31} 22S/(22S + 22R) hopane ratios.

The methylphenanthrene distribution fractions (MDBF), i.e., F_1 = (3-MP + 2-MP)/(1-MP + 2-MP + 3-MP + 9-MP) and F_2 = 2-MP/(1-MP + 2-MP + 3-MP + 9-MP), were proposed by Kvalheim et al. (1987) as effective maturity parameters for coals. Fig. 9c,d illustrates that DNFR values for these coals both exhibit overall increases with increasing F_1 and F_2 values, which can be divided into two parts. The DNFR values for the coals remain at a low constant value at F_1 = 0.14–0.5 and F_2 = 0.09–0.25 (< 1.0 %Ro). Interestingly, DNFR values then gradually increase with increasing F_1 and F_2 values (F_1 > 0.5 and F_2 > 0.25) after peak oil generation (> 1.0 %Ro). The observed phenomena are similar to the trend of DNFR values with increasing vitrinite reflectances. Therefore, DNFR has good correlations with widely used maturity parameters, suggesting that it is a useful maturity indicator for quantitatively assessing thermal maturity.

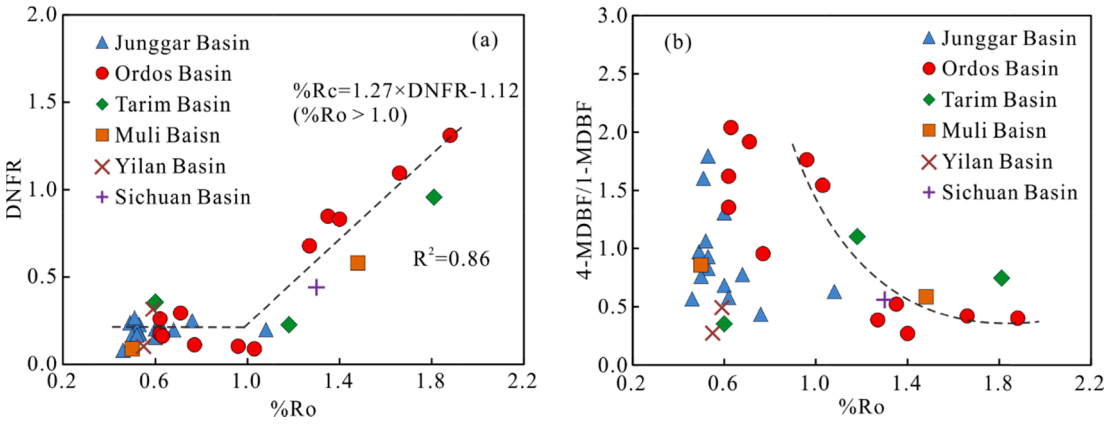

Fig. 8. Correlations of (a) DNFR, (b) 4-MDBF/1-MDBF and vitrinite reflectance of the coals.

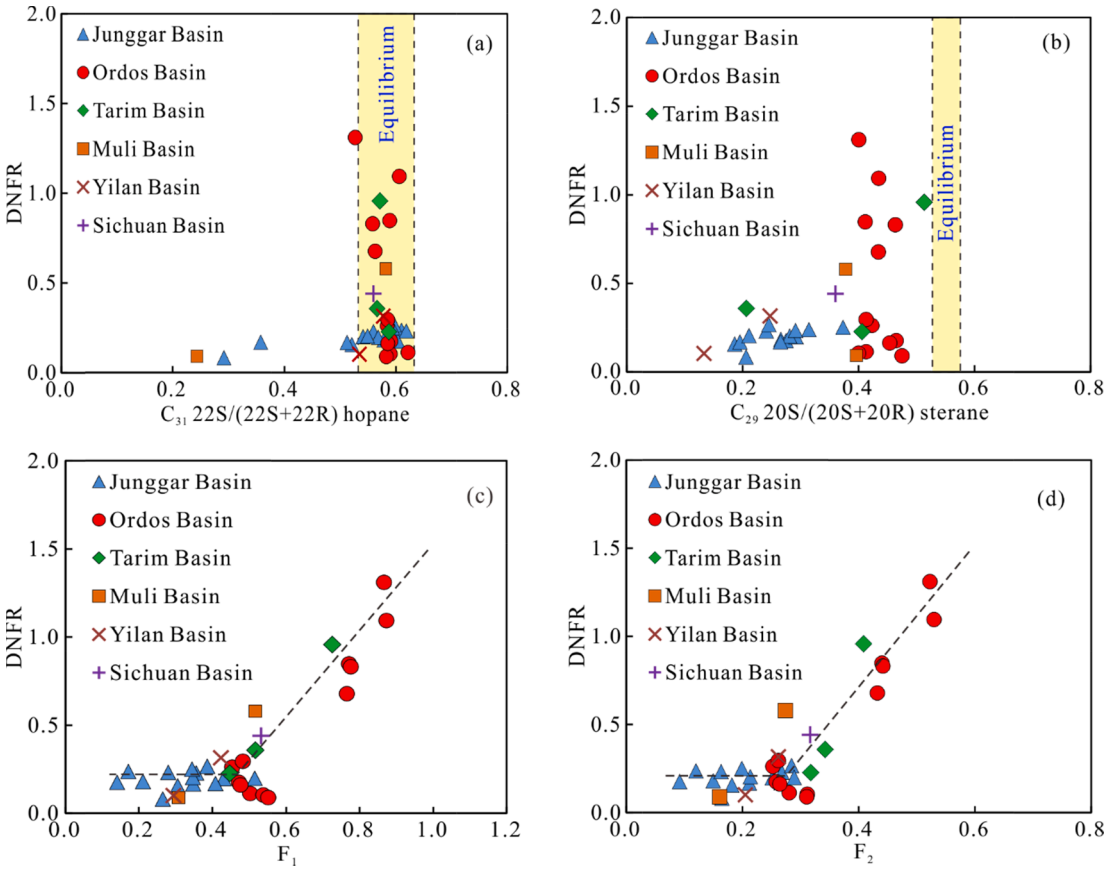

Fig. 9. Correlations of: (a) C_{31} 22S/(22S + 22R) hopane, (b) C_{29} 20S/(20S + 20R) sterane, (c) F_1, (d) F_2 and DNFR of the coals.

4.6. Comparison of the distribution patterns of dinaphthofurans and dibenzofurans

We compared the distributions patterns of the DNFs and dibenzofurans (DBFs) to better understand the formation mechanism of DNFs in the geosphere. The application of 4-MDBF/1-MDBF in evaluating the maturity of source rocks and oils remains a controversial issue. Radke et al. (2000) proposed that 1-MDBF is less stable than 4-MDBF and suggested that the 1-MDBF/4-MDBF ratio can be used as a maturity indicator. However, Li et al. (2011, 2018) found that 1-MDBF/4-MDBF values have no obvious trend with increasing thermal maturity. Fig. 8b shows a comparison of 1221DNF/1223DNF (DNFR) and 4-MDBF/1-MDBF values to vitrinite reflectances. The 4-MDBF/1-MDBF values of the coals display a general decrease with the increase of thermal maturity, which consists of two parts. No obvious regular trend for 4-MDBF/1-MDBF with an increase of thermal maturity within the range of %Ro = 0.46–0.77 was found. However, the 4-MDBF/1-MDBF values of the coals gradually decrease with the increase of thermal maturity after %Ro = 0.96, which is different from the observations reported by previous studies (Radke et al., 2000; Li et al., 2011, 2018). This suggests that thermal maturity is not the key factor controlling the distribution of 1-MDBF and 4-MDBF. In contrast to the 4-MDBF/1-MDBF ratios, the 1221DNF/1223DNF ratios of coals remain constant with % Ro < 1.0, and then display a general increase with the increase of thermal maturity. The result indicates that the behavior of MDBFs is different from DNFs with increasing thermal maturity. This may be

attributed to differences in their formation mechanisms.

Dibenzofuran and methyldibenzofurans are useful molecular markers applied in reflecting sedimentary environment, assessing organic matter type (e.g., Pu et al., 1991; Radke et al., 2000; Li et al., 2013; Li and Ellis, 2015), and tracing oil migration orientation (Li et al., 2011; Li and Ellis, 2015). However, the specific origins of DBFs in petroleum and sedimentary rocks still remain controversial. Previous studies suggested dibenzofurans may be derived from polysaccharides, phenols, or ligneous plants (Born et al., 1989; Pastorova et al., 1994; Sephton et al., 1999; Fenton et al., 2007). Radke et al. (2000) thought dibenzofurans in sedimentary rocks may be derived from lichens. However, laboratory experiments and geochemical observations demonstrate dibenzofurans in sedimentary organic matter and petroleum have an origin from biphenyl compounds (Asif et al., 2010). We combined the absolute concentrations of DBFs and DNFs with the Pr/Ph values to investigate the formation conditions of DBFs and DNFs since the Pr/Ph ratio is a widely used parameter to indicate redox condition of depositional environment (Didyk et al., 1978; Hughes, 1995).

Fig. 10a showed that most coals with low Pr/Ph values (< 1.47) are characterized by high absolute concentrations of DBFs (0.15–4.66 μg/g C_{org}). On the contrary, most of the samples have high Pr/Ph values (2.13–10.3) and extremely low absolute concentrations of DBFs (≤0.06 μg/g C_{org}). There is no clear relationship between the absolute DBFs concentrations and Pr/Ph values of the coal samples. It has been proposed that an oxic environment is conducive to the formation of DBFs (Li and Ellis, 2015; Pu et al., 1991; Radke et al., 2000), which is inconsistent with the observations of this study. However, DNFs behave differently from DBFs with increasing oxic condition. The absolute DNFs concentrations exhibit an overall increase with increasing Pr/Ph values in the coals from the Junggar Basin with %Ro < 0.76. This suggests that oxic conditions contribute to the formation of DNFs at low thermal maturities. Up to now, the formation mechanism of DNFs is not clear, but we have preliminarily observed the difference of DBFs and DNFs under different generating environment and their changes with increasing maturity.

4.7. Origin of the dinaphthofurans in coals

The origin of DNFs in sedimentary organic matter remains a controversial issue. Marynowski et al. (2009) suggested that DNFs may be derived from combustion processes due to their significant concentrations in charcoal-bearing sedimentary sequences related to widespread wildfires. High concentrations of DNFs were found in marine black shales from the Holy Cross Mountains of Poland, which were affected by hydrothermal oxidation (Marynowski et al., 2011). Interestingly, a previous study documented that the concentrations of DNFs in shales altered by hot aqueous fluids are extremely low (Grafka et al., 2015). However, in our study, the coal samples collected in the Junggar Basin have significant concentrations of DNFs without the influence of hydrothermal fluid alteration and combustion processes. Furthermore, the concentrations of DNFs are very low in the coals from the Ordos Basin, which were influenced by hydrothermal oxidation. These observations suggest that the formation of DNFs may not be significantly controlled by hydrothermal oxidation and combustion processes. Specially, most samples investigated by Marynowski et al. (2009, 2011) had a low thermal maturity (< 0.59 %Ro), while those samples analysed by Grafka et al. (2015) were highly mature (> 1.42 %Ro). This suggests that the concentration of DNFs may be mainly controlled by thermal maturity.

In this study, we investigated the relationship between absolute DNFs concentrations and vitrinite reflectances to discuss the origin of DNFs by the comparison of DBFs. The absolute concentrations of DBFs are quite low (≤0.07 μg/g C_{org}) in the coals with %Ro ≤ 0.60, and then follow a rapid increase at %Ro = 0.6–1.0, corresponding to the stage of hydrocarbon generation (Fig. 11a). Interestingly, the absolute concentrations of DBFs rapidly decrease with the increase of thermal maturity after %Ro = 1.0. This suggests that DBFs in sedimentary organic matter may be generated during the diagenesis stage and are the intermediate of forming more condensed aromatic hydrocarbons during high maturity stage. However, with the increase of thermal maturity, the behavior of DNFs is different from that of DBFs. DNFs are present in high absolute concentrations in the coals with low thermal maturities (%Ro < 0.77). With the increase in thermal maturity, the absolute concentrations of DNFs generally decrease at high thermal maturity (%Ro = 0.96–1.88). This indicates that the formation of DNFs probably occurred before the early stage of catagenesis (< 0.77 %Ro). Thermal degradation may cause the decrease of the DNFs concentrations after %Ro = 0.96. This suggests that the DNFs may be derived from diagenetic and catagenetic processes and are more likely degraded or transferred to other compounds at high thermal maturity. Certainly, more work needs to be done to better understand the formation mechanism of DNFs in the geosphere.

5. Conclusions

All six dinaphthofuran isomers have been firmly identified in these coals through co-injection of their authentic standards. Judging from these thermodynamic properties, the stability sequence of DNFs is as follows: 1221DNF > 1212DNF > 1223DNF > 2123DNF > 2323DNF > 2112DNF. The DNF isomers are present in all coals in this study. The less mature coals (%Ro < 1.08) contain 1223DNF as the dominant isomer with low abundances of the other DNF isomers. The relative abundance of 1221DNF compared to 1223DNF exhibits a general increase with the increase of thermal maturity in high maturation stage (%Ro > 1.08). On the basis of the theoretically calculated thermodynamic stabilities and the distribution patterns of DNFs in the coals, a maturity indicator 1221DNF/1223DNF (defined as DNFR) is proposed, which is useful for

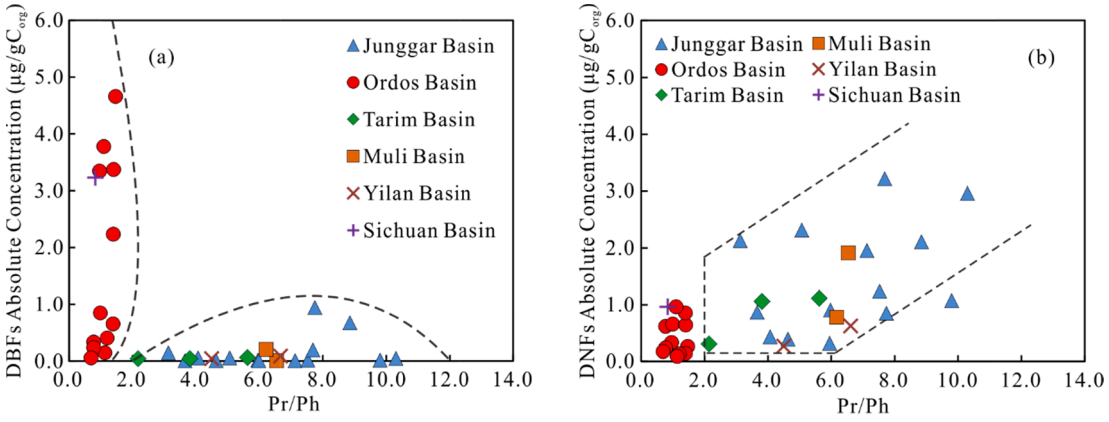

Fig. 10. Correlations of: (a) the absolute concentration of DBFs, (b) the absolute concentration of DNFs and Pr/Ph of the coals.

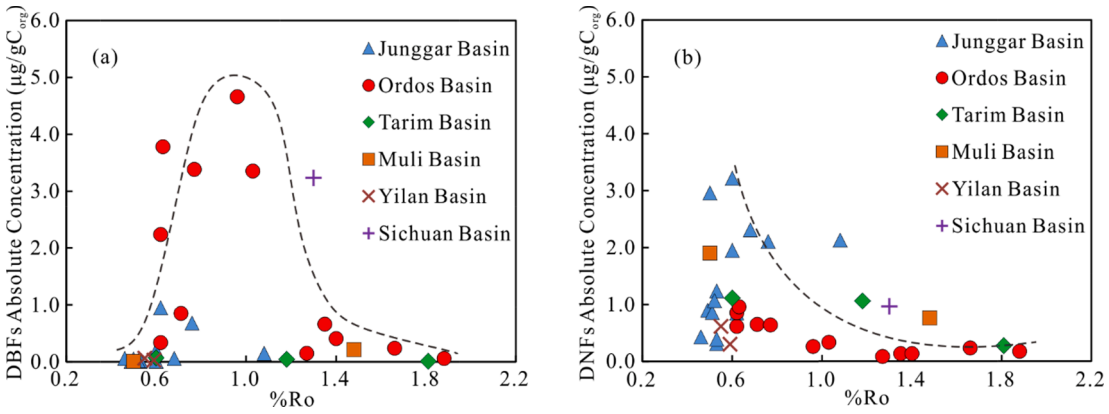

Fig. 11. Correlations of: (a) the absolute concentration of DBFs, (b) the absolute concentration of DNFs and vitrinite reflectance of the coals.

maturity evaluation at high maturity stages. A preliminary calibration of DNFR against the vitrinite reflectance was established as follows: %Rc = 1.27 × DNFR – 1.12 (for %Ro > 1.0) and the correlation coefficients is up to 0.86. DNFs in coals may originate from diagenesis/catagenesis and oxic condition contributes to their formation. This study helps us have a better understanding of the occurrence and distribution patterns of dinaphthofurans in sedimentary organic matter.

Declaration of Competing Interest

The authors declare that they have no known competing financial interests or personal relationships that could have appeared to influence the work reported in this paper.

Acknowledgements

This study was financially supported by the National Natural Science Foundation of China (Grant No. 41972148), the State Key Laboratory of Shale Oil and Gas Enrichment Mechanisms and Effective Development, Beijing (Grant No. 33550007-21-ZC0613-0016), and the National Key Research and Development Program of China (Grant No. 2017YFC0603102). We would like to present our appreciation to Lei Zhu and Shengbao Shi for their help in GC–MS analysis. The authors are grateful to Sichuan University of Science and Engineering for providing computational assistance. We would like to extend our appreciation to the editors Dr. John Volkman Dr Kliti Grice and anonymous reviewers for their constructive suggestions and comments which improved the final paper.

References

Asif, M., Alexander, R., Fazeelat, T., Grice, K., 2010. Sedimentary processes for the geosynthesis of heterocyclic aromatic hydrocarbons and fluorenes by surface reactions. Organic Geochemistry 41, 522–530.

Born, J.G.P., Louw, R., Mulder, P., 1989. Formation of dibenzodioxins and dibenzofurans in homogenous gas–phase reactions of phenols. Chemosphere 19, 401–406.

Borwitzky, H., Schomburg, G., 1979. Separation and identification of polynuclear aromatic compounds in coal tar by using glass capillary chromatography including combined gas chromatography–mass spectrometry. Journal of Chromatography A 170, 99–124.

Brack, W., Klamer, H.J., López de Alda, M., Barceló, D., 2007. Effect-directed analysis of key toxicants in European river basins a review. Environmental Science and Pollution Research 14, 30–38.

Brack, W., Kind, T., Hollert, H., Schrader, S., Möder, M., 2003. Sequential fractionation procedure for the identification of potentially cytochrome P4501A-inducing compounds. Journal of Chromatography A 986, 55–66.

Brack, W., Schirmer, K., 2003. Effect-directed identification of oxygen and sulfur heterocycles as major polycyclic aromatic cytochrome P4501A-inducers in a contaminated sediment. Environmental Science & Technology 37, 3062–3070.

Brack, W., Schirmer, K., Erdinger, L., Hollert, H., 2005. Effect-directed analysis of mutagens and ethoxyresorufin-O-deethylase inducers in aquatic sediments. Environmental Toxicology and Chemistry 24, 2445. https://doi.org/10.1897/05-078R.1.

Chen, J., Liang, D., Wang, X., Zhong, N., Song, F., Deng, C., Shi, X., Jin, T., Xiang, S., 2003. Mixed oils derived from multiple source rocks in the Cainan oilfield, Junggar Basin, Northwest China. Part I: genetic potential of source rocks, features of biomarkers and oil sources of typical crude oils. Organic Geochemistry 34, 889–909.

Dai, J., Li, J., Luo, X., Zhang, W., Hu, G., Ma, C., Guo, J., Ge, S., 2005. Stable carbon isotope compositions and source rock geochemistry of the giant gas accumulations in the Ordos Basin, China. Organic Geochemistry 36, 1617–1635.

Didyk, B.M., Simoneit, B.R.T., Brassell, S.C., Eglinton, G., 1978. Organic geochemical indicators of palaeoenvironmental conditions of sedimentation. Nature 272, 216–222.

Fang, Y., Wu, C., Guo, Z., Hou, K., Dong, L., Wang, L., Li, L., 2015. Provenance of the southern Junggar Basin in the Jurassic: Evidence from detrital zircon geochronology and depositional environments. Sedimentary Geology 315, 47–63.

Fenton, S., Grice, K., Twitchett, R., Bottcher, M., Looy, C., Nabbefeld, B., 2007. Changes in biomarker abundances and sulfur isotopes of pyrite across the Permian-Triassic (P/Tr) Schuchert Dal section (East Greenland). Earth and Planetary Science Letters 262, 230–239.

Feng, C., Zou, H., Guo, T., Zhu, Y., 2013. Evaluation of source rocks in Upper Permian Wujiaping Formation of Northeast Sichuan and its adjacent area. Journal of Earth Science and Environment 35, 18–29 (in Chinese with English abstract).

Grafka, O., Marynowski, L., Simoneit, B.R.T., 2015. Phenyl derivatives of polycyclic aromatic compounds as indicators of hydrothermal activity in the Silurian black siliceous shales of the Bardzkie Mountains, Poland. International Journal of Coal Geology 139, 142–151.

Guseva, G.M., Kolokolov, B.N., Khmel'nitskii, R.A., 1980. Determination of impurities in technical 2-naphthol by mass spectrometry and IR spectroscopy. Journal of Organic Chemistry of the USSR 16, 141–146.

Hendrix, M.S., Brassell, S.C., Carroll, A.R., Graham, S.A., 1995. Sedimentology, organic geochemistry, and petroleum potential of Jurassic coal measures: Tarim, Junggar, and Turpan basins, northwest China. American Association of Petroleum Geologists Bulletin 79, 929–959.

Hu, G., Li, J., Shan, X., Han, Z., 2010. The origin of natural gas and the hydrocarbon charging history of the Yulin gas field in the Ordos Basin, China. International Journal of Coal Geology 81, 381–391.

Huang, S., Fang, X., Liu, D., Fang, C., Huang, T., 2015. Natural gas genesis and sources in the Zizhou gas field, Ordos Basin, China. International Journal of Coal Geology 152, 132–143.

Hughes, W.B., Holba, A.G., Dzou, L.I.P., 1995. The ratios of dibenzothiophene to phenanthrene and pristane to phytane as indicators of depositional environment and lithology of petroleum source rocks. Geochimica et Cosmochimica Acta 59, 3581–3598.

Kilby, W.E., 1988. Recognition of vitrinite with non-uniaxial negative reflectance characteristics. International Journal of Coal Geology 9, 267–285.

Kováts, E., 1958. Gas-chromatographische Charakterisierung organischer Verbindungen. Teil 1: Retentionsindices aliphatischer Halogenide, Alkohole. Aldehyde und Ketone. Helvetica Chimica Acta 41, 1915–1932.

Kruge, M.A., 2000. Determination of thermal maturity and organic matter type by principal components analysis of the distributions of polycyclic aromatic compounds. International Journal of Coal Geology 43, 27–51.

Kvalheim, O.M., Christy, A.A., Telnæs, N., Bjørseth, A., 1987. Maturity determination of organic matter in coals using the methylphenanthrene distribution. Geochimica et Cosmochimica Acta 51, 1883–1888.

Lee, M.L., Vassilaros, D.L., White, C.M., Novotny, M., 1979. Retention indices for programmed-temperature capillary-column gas chromatography of polycyclic aromatic hydrocarbons. Analytical Chemistry 51, 768–773.

Li, D., Liang, D., Jia, C., Wang, G., Wu, Q., He, D., 1996. Hydrocarbons accumulations in the Tarim Basin, China. American Association of Petroleum Geologists Bulletin 80, 1587–1603.

Li, J., Zhuang, X., Querol, X., Font, O., Moreno, N., Zhou, J., Lei, G., 2012a. High quality of Jurassic Coals in the Southern and Eastern Junggar Coalfields, Xinjiang, NW China: Geochemical and mineralogical characteristics. International Journal of Coal Geology 99, 1–15.

Li, M., Ellis, G.S., 2015. Qualitative and quantitative analysis of dibenzofuran, alkyldibenzofurans, and benzo[b]naphthofurans in crude oils and source rock extracts. Energy & Fuels 29, 1421–1430.
Li, M., Gao, JianRong, 2010. Basement faults and volcanic rock distributions in the Ordos Basin. Science China-Earth Sciences 53, 1625–1633.
Li, M., Shi, S., Wang, T.-G., 2012b. Identification and distribution of chrysene, methylchrysenes and their isomers in crude oils and rock extracts. Organic Geochemistry 52, 55–66.
Li, M., Wang, T., Yang, F., Shi, Y., 2011. Molecular tracers for filling pathway in condensate pools: Alkyldibenzofuran. Journal of Oil and Gas Technology 33, 6–11 in Chinese with English abstract.
Li, M., Zhong, N., Shi, S., Zhu, L., Tang, Y., 2013. The origin of trimethyldibenzothiophenes and their application as maturity indicators in sediments from the Liaohe Basin, East China. Fuel 103, 299–307.
Liang, D., Zhang, S., Chen, J., Wang, F., Wang, P., 2003. Organic geochemistry of oil and gas in the Kuqa depression, Tarim Basin, NW China. Organic Geochemistry 34, 873–888.
Liao, J., Lu, H., Sheng, G., Peng, P., Hsu, C.S., 2015. Monoaromatic, diaromatic, triaromatic, and tetraaromatic hopanes in Kukersite shale and their stable carbon isotopic composition. Energy & Fuels 29, 3573–3583.
Liu, B., Lü, Y., Zhao, R., Tu, X., Guo, X., Shen, Y., 2012a. Formation overpressure and shale oil enrichment in the shale system of Lucaogou Formation, Malang Sag, Santanghu Basin, NW China. Petroleum Exploration and Development 39, 744–750.
Liu, R., Liu, Z., Liu, S., Liu, D., Li, B., Yang, X., Xu, Y., 2012b. Coal and oil occurrence characteristics and metallogenic regularity in Yilan Basinn. Journal of China Coal Society 37, 776–781 in Chinese with English abstract.
Liu, X., Li, M., Zhang, C., Fang, R., Zhong, N., Xue, Y., Zhou, Y., Jiang, W., Chen, X., 2020. Mechanistic insight into the optimal recovery efficiency of CBM in sub-bituminous coal through molecular simulation. Fuel 266, 117–137.
Lübcke-von Varel, U., Streck, G., Brack, W., 2008. Automated fractionation procedure for polycyclic aromatic compounds in sediment extracts on three coupled normal-phase high-performance liquid chromatography columns. Journal of Chromatography A 1185, 31–42.
Marynowski, L., Simoneit, B.R.T., 2009. Widespread Upper Triassic to Lower Jurassic wildfire records from Poland: Evidence from charcoal and pyrolytic polycyclic aromatic hydrocarbons. Palaios 24, 785–798.
Marynowski, L., Kurkiewicz, S., Rakociński, M., Simoneit, B.R.T., 2011. Effects of weathering on organic matter: I. Changes in molecular composition of extractable organic compounds caused by paleoweathering of a Lower Carboniferous (Tournaisian) marine black shale. Chemical Geology 285, 144–156.
Nytoft, H.P., Vuković, N.S., Kildahl-Andersen, G., Rise, F., Životić, D.R., Stojanović, K.A., 2016. Identification of a novel series of benzohopanes and their geochemical significance. Energy & Fuels 30, 5563–5575.
Pastorova, I., Botto, R.E., Arisz, P.W., Boon, J.J., 1994. Cellulose char structure: a combined analytical Py–GC–MS, FTIR, and NMR study. Carbohydrate Research 262, 27–47.
Peters, K.E., Moldowan, J.M., Sundararaman, P., 1990. Effects of hydrous pyrolysis on biomarker thermal maturity parameters: Monterey phosphatic and siliceous members. Organic Geochemistry 15, 249–265.
Peters, K.E., Walters, C.C., Moldowan, J.M., 2005. The Biomarker Guide: Volume 2, Biomarkers and Isotopes in Petroleum Systems and Earth History. Cambridge University Press.
Poutsma, M.L., Dyer, C.W., 1982. Thermolysis of model compounds for coal. 2. Condensation and hydrogen transfer during thermolysis of naphthols. Journal of Organic Chemistry 47, 3367–3377.
Pu, F., Philp, R.P., Li, Z., Yu, X., Ying, G., 1991. Biomarker distributions in crude oils and source rocks from different sedimentary environments. Chemical Geology 93, 61–78.
Qian, Y.u., Zhang, T., Wang, Z., Tuo, J., Zhang, M., Wu, C., Tian, C., 2018. Organic geochemical characteristics and generating potential of source rocks from the Lower-Middle Jurassic coal-bearing strata in the East Junggar Basin, NW China. Marine and Petroleum Geology 93, 113–126.
Radke, M., Vriend, S.P., Ramanampisoa, L.R., 2000. Alkyldibenzofurans in terrestrial rocks: Influence of organic facies and maturation. Geochimica et Cosmochimica Acta 64, 275–286.
Rospondek, M.J., Marynowski, L., Chachaj, A., Góra, M., 2009. Novel aryl polycyclic aromatic hydrocarbons: Phenylphenanthrene and phenylanthracene identification, occurrence and distribution in sedimentary rocks. Organic Geochemistry 40, 986–1004.
Sephton, M.A., Looy, C.V., Veefkind, R.J., Visscher, H., Brinkhuis, H., de Leeuw, J.W., 1999. Cyclic diaryl ethers in a Late Permian sediment. Organic Geochemistry 30, 267–273.
Seifert, W.K., Moldowan, J.M., 1980. The effect of thermal stress on source-rock quality as measured by hopane stereochemistry. Physics and Chemistry of the Earth 12, 229–237.
Seifert, W.K., Moldowan, J.M., 1986. Use of biological markers in petroleum exploration. Methods in Geochemistry and Geophysics 24, 261–290.
Shuai, Y., Zhang, S., Mi, J., Gong, S., Yuan, X., Yang, Z., Liu, J., Cai, D., 2013. Charging time of tight gas in the Upper Paleozoic of the Ordos Basin, central China. Organic Geochemistry 64, 38–46.
Shultz, J.L., Kessler, T., Friedel, R.A., Sharkey, A.G., 1972. High-resolution mass spectrometric investigation of heteroatom species in coal-carbonization products. Fuel 51, 242–246.
Skoczyńska, E., Korytár, P., de Boer, J., 2008. Maximizing chromatographic information from environmental extracts by GC×GC–ToF–MS. Environmental Science & Technology 42, 6611–6618.
Stock, L.M., Obeng, M., 1997. Oxidation and decarboxylation. A reaction sequence for the study of aromatic structural elements in Pocahontas No. 3 coal. Energy & Fuels 11, 987–997.
Tenger, Qin, J., Fu, X., Yang, Y., Xie, X., 2013. Hydrocarbon source rocks evaluation of the Upper Permian Wujiaping Formation in northeastern Sichuan area. Journal of Palaeogeography 12, 334–345 (in Chinese with English abstract).
van Den Dool, H., Kratz, P.D., 1963. A generalization of the retention index system including linear temperature programmed gas-liquid partition chromatography. Journal of Chromatography A 11, 463–471.
van Duin, A.C.T., Baas, J.M.A., van de Graaf, B., de Leeuw, J.W., Bastow, T.P., Alexander, R., 1997. Comparison of calculated equilibrium mixtures of alkylnaphthalenes and alkylphenanthrenes with experimental and sedimentary data; the importance of entropy calculations. Organic Geochemistry 26, 275–280.
Vondráček, J., Chramostová, K., Plíšková, M., Bláha, L., Brack, W., Kozubík, A., Machala, M., 2004. Induction of aryl hydrocarbon receptor–mediated and estrogen receptor–mediated activities, and modulation of cell proliferation by dinaphthofurans. Environmental Toxicology and Chemistry 23, 2214. https://doi.org/10.1897/03-620.
Wang, D., Li, Z., Wang, Z., Lu, D., Liu, H., Wang, P., Zheng, X., Lu, Y., Li, X., 2013. Paleogene coal and oil shale paragenetic features and sequence stratigraphic framework in Yilan Basin, Heilongjiang. Coal Geology of China 25, 1–7 in Chinese with English abstract.
Wang, N., Li, M., Liu, X., Hong, H., Tian, X., Yang, C., Shi, S., Liu, P., 2020. Geo-chromatographic fractionation effect of methyldibenzofuran in dolomite reservoirs and its application in tracing oil filling pathways in the Sichuan Basin. Marine and Petroleum Geology 113, 104126. https://doi.org/10.1016/j.marpetgeo.2019.104126.
Xiao, H., Krauss, M., Floehr, T., Yan, Y., Bahlmann, A., Eichbaum, K., Brinkmann, M., Zhang, X., Yuan, X., Brack, W., Hollert, H., 2016. Effect-directed analysis of aryl hydrocarbon receptor agonists in sediments from the Three Gorges Reservoir, China. Environmental Science & Technology 50, 11319–11328.
Xiao, H., Li, M., Wang, W., You, B., Liu, X., Yang, Z., Liu, J., Chen, Q., Uwiringiyimana, M., 2019. Identification, distribution and geochemical significance of four rearranged hopane series in crude oil. Organic Geochemistry 138, 103929. https://doi.org/10.1016/j.orggeochem.2019.103929.
Xu, X., Shao, L., Zhang, F., Huang, M., Ju, Q., Wen, H., Wang, W., Lu, J., 2011. Sequence stratigraphy and coal accumulation of the Jurassic in Wailihada mining area of Muli coalfield in Qinghai Province. Journal of Palaeogeography 13, 317–324 in Chinese with English abstract.
Yang, L., Li, M., Wang, T.-G., Liu, X., Jiang, W., Fang, R., Lai, H., 2017. Phenyldibenzofurans and methyldibenzofurans in source rocks and crude oils, and their implications for maturity and depositional environment. Energy & Fuel 31, 2513–2523.
Yang, S., Li, M., Liu, X., Han, Q., Wu, J., Zhong, N., 2019. Thermodynamic stability of methyldibenzothiophenes in sedimentary rock extracts: Based on molecular simulation and geochemical data. Organic Geochemistry 129, 24–41.
Yang, Y., Li, W., Ma, L., 2005. Tectonic and stratigraphic controls of hydrocarbon systems in the Ordos Basin: a multicycle cratonic basin in central China. American Association of Petroleum Geologists Bulletin 89, 255–269.
Zhang, D., 1996. Sandstone-type kaoline deposit in Jurassic coal measures strata, Datong mining area, Qinghai Province. Coal Geology of China 18, 37–41 in Chinese with English abstract.
Zhou, J., Zhuang, X., Alastuey, A., Querol, X., Li, J., 2010. Geochemistry and mineralogy of coal in the recently explored Zhundong large coal field in the Junggar Basin, Xinjiang province, China. International Journal of Coal Geology 82, 51–67.
Zhu, G., Wang, T., Xie, Z., Xie, B., Liu, K., 2015. Giant gas discovery in the Precambrian deeply buried reservoirs in the Sichuan basin, China: implications for gas exploration in old cratonic basins. Precambrian Research 262, 45–66.
Zhu, Z., Li, M., Tang, Y., Qi, L., Leng, J., Liu, X., Xiao, H., 2019. Identification of phenyldibenzothiophenes in coals and the effects of thermal maturity on their distributions based on geochemical data and theoretical calculations. Organic Geochemistry 138, 103910. https://doi.org/10.1016/j.orggeochem.2019.103910.
Zou, C., Wei, G., Xu, C., Du, J., Xie, Z., Wang, Z., Hou, L., Yang, C., Li, J., Yang, W., 2014. Geochemistry of the Sinian-Cambrian gas system in the Sichuan Basin, China. Organic Geochemistry 74, 13–21.